INTERNATIONAL JOURNAL of RENEWABLE ENERGY RESEARCH
A. S. Cherif et al., Vol.16, No.2, June, 2026

Thermal and Energy Performances Analysis of Overheated Educational Space Based on Data Driven Approach

Amel Soukaina Cherif*, Sondes Skander-Mustapha **‡, Ilhem Slama Belkhodja***

*Université Carthage, Ecole Nationale d'Architecture et d'Urbanisme, 2026 Sidi Bou Said, LETTM (LR01ES07), Université de Tunis El Manar, Faculté des Sciences de Tunis, 1002, Tunis, Tunisie
** Université Carthage, Ecole Nationale d'Architecture et d'Urbanisme, 2026 Sidi Bou Said, LSE (LR11ES15), Université de Tunis El Manar, Ecole Nationale d'Ingénieurs de Tunis, 1002, Tunis, Tunisie.
*** Université Tunis El Manar, Ecole Nationale d'Ingénieurs de Tunis, LES (LR11ES15), 1002, Tunis, Tunisie.
(amelsoukeina.cherif@enau.ucar.tn, sondes.skander@enit.utm.tn, ilhem.slamabelkhodja@enit.utm.tn)

‡Corresponding Author; Sondes Skander-Mustapha, ENAU, 2026 Sidi Bou Said, Tel: +216 97 711 790, sondes.skander@enit.utm.tn

Received: 22.02.2024 Accepted: 08.04.2024

Abstract- This study addresses the critical issue of overheating in built environments. With increasing extreme heat events and dense urbanization, overheating poses serious risks to human health, productivity, and well-being. Existing research mainly emphasizes external environmental drivers, leaving a gap in understanding internal building dynamics. This paper examines the thermal and energy behavior of an overheated educational laboratory room, pursuing two objectives: defining indoor comfort temperatures to enhance productivity and evaluating energy consumption to identify potential savings. A detailed numerical model of the laboratory envelope, incorporating interior electrical loads and air-conditioning systems, is developed using data from a monitoring setup that captures dynamic temperature variations. By applying the Narxnet predictive algorithm to historical temperature and humidity data, the model estimates energy consumption with high accuracy. Key challenges included creating a reliable model that reflects the complexity of the space, building a robust prediction method, and accurately representing air-conditioning use. The technical approaches adopted to address these issues are presented, offering insights applicable to other overheated buildings. Results extend beyond the specific case, contributing to broader strategies for mitigating overheating. Validation confirms strong performance, with a 2% prediction error and less than 1°C deviation in the envelope model, except for the glass façade, which reaches 1°C. Estimated cooling demand also confirms the adequacy of the installed photovoltaic system, even under curtailment conditions, ensuring reliable and efficient operation.

Keywords Overheated space, envelope thermal behaviour, energy-consumption prediction, internal generating heat, photovoltaic panel, narxnet modelling.

1. Introduction

The growing demand for energy is one of the main drivers of resource scarcity and environmental degradation. In order to ensure energy security while meeting environmental requirements, activities with negative impacts must be carefully controlled and optimized. In this context, the building sector represents one of the largest consumers of energy, making its optimization essential for improving overall energy efficiency and reducing environmental impacts.

Several studies focus on the prevention of energy overconsumption in buildings by acting on the envelope as well as on air-conditioning or heating systems. The applied strategies differ according to building categories, commercial [1], residential [2,3], office [4,5], or educational buildings [6].

In the literature, approaches to achieving building energy efficiency vary depending on the studied parameters. Researchers have focused on improving energy performance

through building envelope properties [7,8], insulation thickness [9], heating, ventilation, and air-conditioning system performance [8,9] and building occupancy [10].

Researchers diligently ensure optimal indoor environments for inhabited spaces, conducting extensive investigations into the combined or individual effects of architectural [11] and technical choices [12-14], employing optimization models and predictive algorithms for regulatory systems [15-18]. However, evaluation suggests that current building energy regulations may not adequately prevent overheating or prepare for warmer conditions, as indicated by [18]. This persistent issue of global energy consumption in the building sector persists despite efforts to mitigate climate change, resulting in discomfort from internal space warming.

Nevertheless, what is striking is that most of the new research focuses on overheating risks stemming from designs or climatic conditions in specific contexts, relying on collected data and measurements to inform their evaluations. Recent studies by authors in [19] and [20] demonstrate that calibrated and validated models offer precise predictions, with enhanced accuracy compared to measured data, highlighting the importance of utilizing real values and parameters for realistic outcomes. Few studies address overheating risks caused by internal factors such as heat-generating appliances. Aiming at lighting and household appliances, authors in [21], assert that control measures adequately mitigate the risk of overheating attributed to internal loads. But when it comes to specific equipment generating a lot of heat through Joule effect and contributing to space overheating, to our knowledge, no work has addressed the overheating coming from within and its consequences on energy consumption.

In this paper, we focused on the most energy-intensive area located in an educational building containing overheating loads. In fact, the installed appliances in this space generate a lot of heat, negatively affect occupants, and disturb their performances. Thus, ensuring comfort requires the continuous operation of the air conditioner. Thereby, the aim is to ensure a comfortable working environment while optimizing air conditioner functioning and achieving its independence from the national electricity grid. The goal was addressed by employing a numerical thermal model that relies on data measured by wireless sensors. Additionally, a predictive algorithm for energy consumption was created using the Narxnet algorithm.

The paper's framework progresses as follows: In Section 2, we delve into the detailed presentation of materials and methods. Section 3 elucidates the proposed model, designed using Matlab/Simscape. A predictive algorithm for data processing and prescriptive outputs for thermal behaviour is given. Section 4 furnishes model validation, where we analyse thermal envelope behaviour, and give predictive heat flow and energy consumption.

2. Material and Method

2.1. Thermophysical and Geometrical Description

For this study a typical laboratory room located on Campus Tunis El Manar at the National Engineering School of Tunis is studied. It is outfitted with heat-producing appliances and equipment. Its total area is 45m² and its occupied volume is 189 m³. The 2D plan, dimensions, and 3D layout are shown in 'Fig. 1,' while the composition of the walls and their thermophysical specifications are shown in "Fig. 2" and "Table 2", respectively.

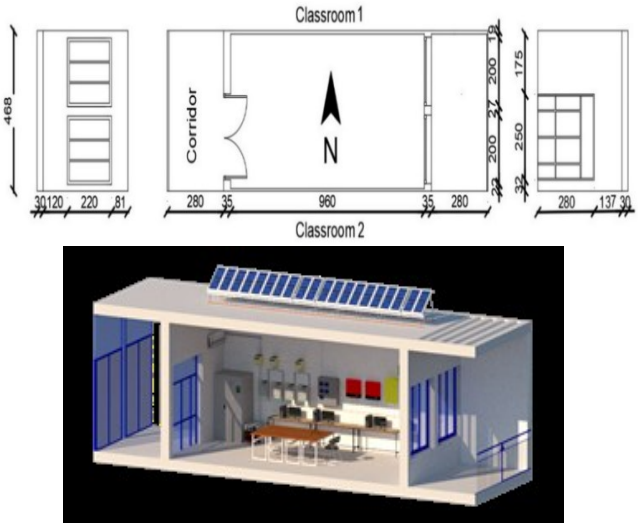

Fig. 1. Laboratory sketching and 3D CAD section model.

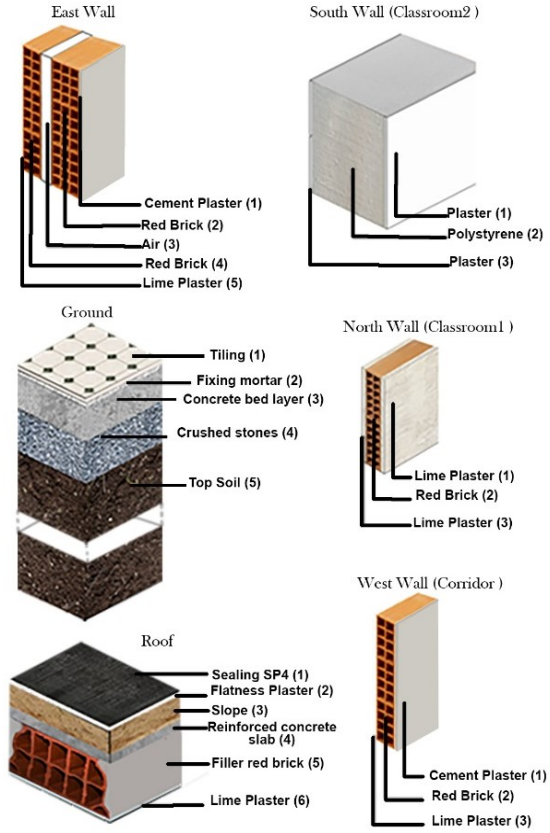

Fig. 2. Composition of the walls.

Table 1. Thermophysical envelope characteristics

	Composition	**e (m)**	**ρ (kg/m³)**	**Cp (J/kg°K)**	**λ (W/mK)**
North Wall	Lime plaster (1)	0.015	1600	1000	0.75
	Red brick (2)	0.07	1950	1100	0.35
	Lime plaster (3)	0.015	1550	1000	0.7
South Wall	Plaster (1)	0.013	825	1450	0.3
	Polystyrene (2)	0.4	32	1450	0.035
	Plaster (3)	0.013	825	1450	0.3
East Wall	Cement plaster (1)	0.015	1900	925	0.85
	Red Brick (2)	0.1	1920	840	0.35
	Air (3)	0.06	1	900	0.280
	Red brick (4)	0.15	1920	840	0.35
	Lime plaster (5)	0.015	1550	840	0.7
West Wall	Cement plaster (1)	0.015	1900	925	0.85
	Red brick (2)	0.1	1920	840	0.35
	Lime plaster (3)	0.015	1550	840	0.7
Roof	Sealing SP4 (1)	0.004	1150	1000	0.230
	Flatness plaster (2)	0.02	1200	1000	0.570
	Slope (3)	0.1	1.4	800	1.10
	Reinforced concrete slab (4)	0.05	2500	878	1.5
	Filler red brick (5)	0.25	1800	1000	0.35
	Lime plaster (6)	0.015	1450	840	0.7
Ground	Tiling (1)	0.02	2400	875	2.4
	Fixing mortar (2)	0.015	1500	850	1.5
	Concrete bed layer (3)	0.15	2500	878	1.5
	Crushed stones (4)	0.20	1800	1000	2
	Top soil (5)	1	1500	1900	0.75

2.2. Experimental Devices and Thermal Data Instrumentation

As presented on "Fig 3", temperatures data are collected using Testo devices:

- The WiFi data logger with two connectable type K thermocouples recorded all detected temperature values and transferred them to the Testo Cloud "Saveris2" every 15 minutes, 24 hours daily. Connected sensors raised both internal and external surfaces of eastern, southern, western, and northern walls components, ground, and roof. They are fixed on the middle of each surface.

- The multifunction Testo 435-4 devices with temperature probes transmitted indoor and outdoor air temperature to a software installed on PC, via an USB connection every 15 minutes, 24 hours daily. The probes are installed at 1.5m high above the ground level.

- A fully autonomous weather station with its photovoltaic panel: GPRS-LT type enabling permanent data recording with retrieval via the GPRS network.

The technical specifications of the experimental devices are summarized on "Table 2".

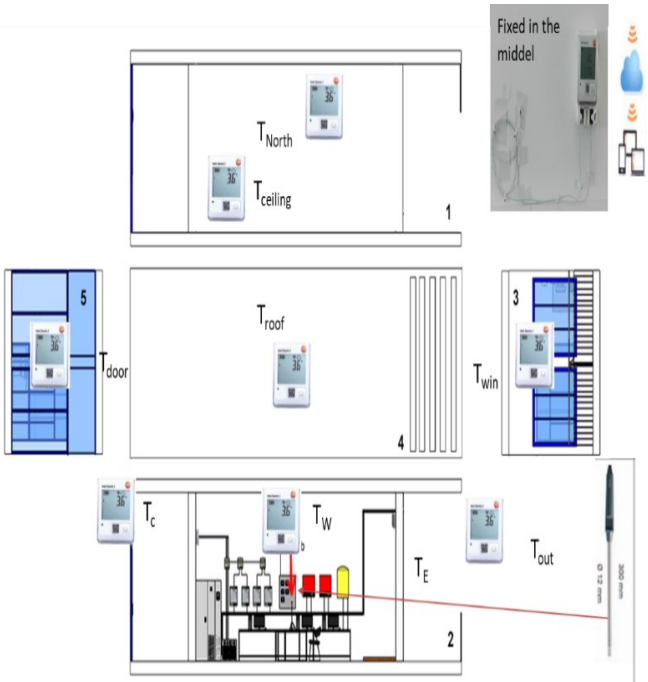

Fig. 3. Measurement's sensors position.

Table 2. Technical specifications of the experimental instrumentation

Type	Range of measurement	Accuracy	Resolution
Multifunction device Testo 435-4 and temperature measuring probe	-20 to +70 °C	±0.3 °C	0.1 °C
Testo Saveris 2-T3 with K-type thermocouples	(-195 to +1350 °C)	±(0.5 + 0.5 % of mv) °C	0.5°C

3. Integrated Data-Driven Framework for Thermal and Energy Management Modelling

A detailed framework that includes data-driven collection is depicted in "Fig. 4." This framework comprises a predictive algorithm for data processing, a room model, and prescriptive outputs for both thermal and energy behaviour. The inputs are provided by experimental temperature measurements recorded every 15 minutes and stored in a cloud via WiFi. The room model includes the envelope subsystem, the scheduled loads according to the load profile which is based on the planned tests in the laboratory by various stakeholders. It is noteworthy that in the general case, the load profile can also be derived from a prediction program, especially in the context of residential or industrial applications and finally, the indoor temperature regulation subsystem, which is achieved through the control of the air conditioner. The processed data temperature and energy consumption are predicted through the physical-based model. The simulated program is designed on the graphical Simscape/ Matlab interface. The details regarding the mathematical model as well as the control system of the air conditioner are given as follows.

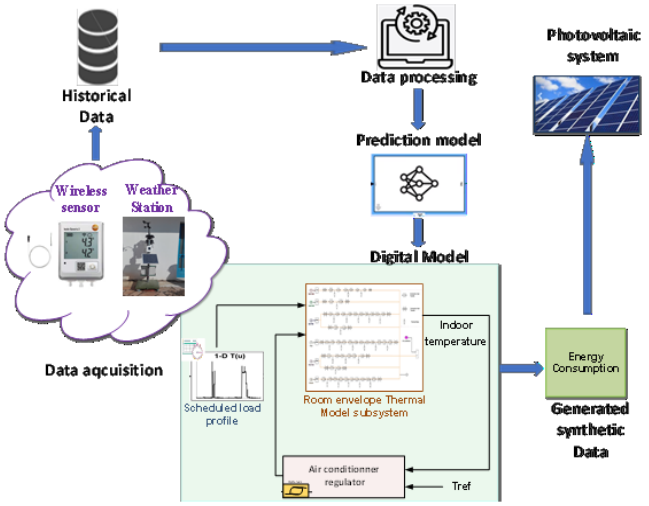

Fig. 4. Laboratory digital model including thermal data and control subsystem.

The thermal behaviour of the laboratory is mainly governed by three factors: the heat exchange with the outside air through its envelope, the energy provided by the air conditioner, and internal heat gains provided by human bodies, appliances, and lighting.

To express the conductive heat transfer through opaque and transparent envelope components, Fourier's law is expressed by "Eq. (1)" and "Eq. (2)" respectively.

$$\Phi_{Cond(ij)} = k\frac{S_w}{d_{ij}}(\Theta_i - \Theta_j) \quad (1)$$

$$\Phi_{win/door} = UMS_{\frac{win}{door}}(\Theta_i - \Theta_{\frac{ext}{corr}}) \quad (2)$$

Where, k is thermal conductivity [Wm $^{-1}$ K $^{-1}$], S_w is wall area [m²], d_{ij} is wall layer's thickness [m], θ_i and θ_j are face i/j temperature respectively[°K].

(U) is the window/door thermal transmittance [W/(m²·K)], *($S_{win/door}$)* is the window area [m²], θ_i and $\theta_{ext/corr}$ are internal/external/corridor temperature respectively[°K].

The convective heat transfer is expressed by Newton law:

$$\Phi_{Conv(in/out)} = K_{S_{in/out}} S_w \Delta\Theta \quad (3)$$

Where, *($K_{s\_in/out}$)* is thermal conductivity, *(S_w)* is wall area [m²], *(d_{ij})* is wall layer's thickness [m], *(θ)* is the temperature [°K]

As a result of the room's mathematical model, the laboratory room envelope subsystem model was built on Matlab Simscape graphical environment. The envelope laboratory room model considers the room as a thermal system which is equivalent to an electric system. The connections in the system are the room elements (walls, openings etc.). Each component is represented by its thermal capacitance and its thermal resistance. The temperature on every point is equivalent to the voltage. The heat flows are analogous to the electric power.

A fine discretization takes into consideration the different envelope layers in order to simulate the dynamic evolution of temperature profiles in various layers.

The following hypotheses are considered:

- Temperature field around the entire room is uniform.

- The temperature measurements are not disturbed.

- Thermal-physical coefficients are independent of temperature.

Internal heat gains by occupants and by electric devices and lighting are given by "Eq. (4)" and "Eq. (5)" respectively.

$$P = n\frac{qt}{24} \quad (4)$$

$$P_{el} = \sum_i p_e\, k_e \quad (5)$$

Where *(n)* is number of occupants, *(q)* is the power released by occupants [kW] and *(t)* is the attendance time in hours per day.

(P_{ei}) is electrical consumed power consumed and (k_e) is correction factor [kW]

Heat storage through the thermal mass of the different materials constituting the envelope and ambiance room is expressed in the "Eq. (6)" and expresses the heat storage room capacity.

$$\Phi_M = CM_{st}\frac{d\Theta}{dt} \quad (6)$$

Where, *(C)* is thermal capacity [J/(kg °K)]and $(m_{s,t})$ is mas [kg], (θ) is the temperature [°K] and *(t)* is the time [h]

In addition to the primary charges expressed by "Eq. (4)" and "Eq. (5)", various secondary loads are activated during laboratory tests and manipulations conducted by researchers. These tests are scheduled with detailed power profiles for the loads to be used. Examples of these scheduled load profiles are illustrated in "Fig. 5". They operate concurrently with occupants present, contributing to unpleasant working conditions due to overheating. Technical specifications for the different loads are provided in "Table 3". Furthermore, the impact of overheating on room temperature in the absence of air conditioning activation is clearly visible in "Fig. 6".

Table 3. Electrical load specifications

Electric overheating devices	Quantity	Unit electrical power
Inverter1	4	3kW
Inverter2	1	7kW
Resistive load	2	4kW
Lighting	6	36W*2
Transformer (currently it is not connected)	1	15kVA

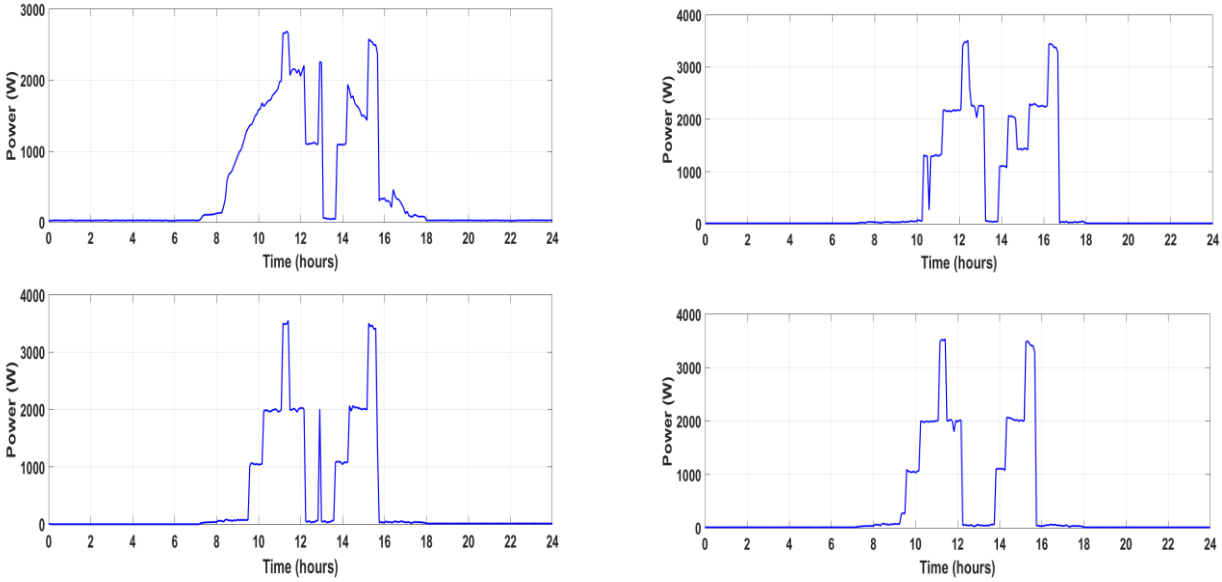

Fig. 5. Examples of scheduled Load tests.

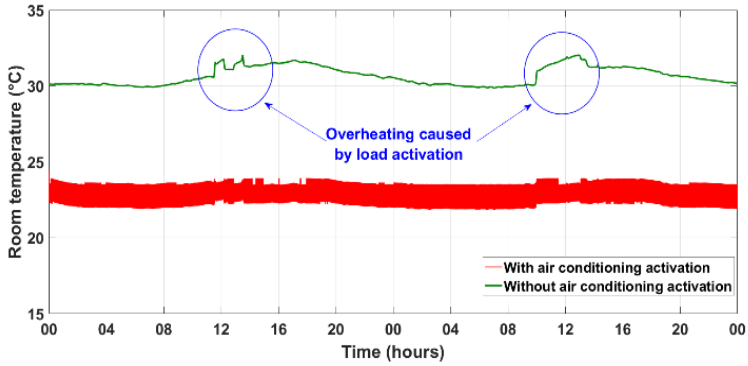

Fig. 6. Indoor temperature dynamics under overheating conditions with and without air conditioning.

The temperature control implemented in the air conditioner regulation subsystem operates on a hysteresis loop utilizing zero-crossing operation. This loop maintains the difference between the room's ambient temperature and the reference value within a well-defined margin. The air conditioning system is activated when the temperature exceeds the upper threshold of its operating range. The hysteresis method is well-suited for this application as it prevents rapid switching between running and stopping cooling units.

4. Results and discussions

4.1. Data-Driven Temperature Prediction

We employed a methodology grounded in data analysis to forecast temperature fluctuations across different walls within the study area. The dataset spans from January 1, 2022, to April 24, 2023, encompassing outdoor temperatures and humidity levels. The prediction model was implemented using Matlab, with the following program outlining the procedure. The temporal information was converted into numeric format for processing. A neural network with one input layer, one feedback layer, and five hidden neurons was constructed using the NARX (Nonlinear Autoregressive with eXogenous input) architecture. The data, consisting of the exterior temperatures for each wall and the corresponding humidity, were prepared for training and simulation. The dataset was divided into training (75%) and testing (25%) sets based on a time-based division. The 'trainlm' algorithm was employed for training the neural network, with performance evaluation and results displayed through performance metrics and response plots. In "Fig. 7", we provide a thorough analysis of the neural network model's performance through four distinct curves representing different datasets. The 'Training' curve, marked by an impressive correlation coefficient (R) of 0.99815, showcases the model's remarkable ability to discern the inherent patterns within the training dataset. Similarly, the 'Validation' curve, with an R value of 0.99803, demonstrates the model's robust generalization to new, unseen data. The 'Test' curve, boasting an R of 0.99781, signifies the model's proficiency in maintaining high predictive accuracy on an independent test dataset. Finally, the 'All' curve, encapsulating the combined information from training, validation, and test datasets, displays a remarkable R of 0.99806, affirming the model's overall strength in capturing the underlying relationships present in the entire dataset. These high correlation coefficients across all datasets suggest that the neural network's predictions closely align with the actual values, emphasizing the model's efficacy in learning and generalizing from the given data.

An example illustrating the comparison between predicted and actual temperatures is presented in "Fig. 8", specifically focusing on the external ambient temperature. In evaluating the performance of the temperature prediction model, we computed the mean relative error, which amounted to approximately 2.1745%. This metric reflects the average percentage difference between the predicted temperatures and the actual values over the entire dataset. Importantly, a mean relative error of this magnitude suggests a relatively small deviation on average. In the context of temperature prediction, where precision is often crucial, this value signifies a commendable level of accuracy. Generally, a mean relative error below 5% is considered acceptable in many applications, and our result falls comfortably within this range. While there are specific instances with higher errors, the overall performance indicates that the model aligns well with the actual temperature trends.

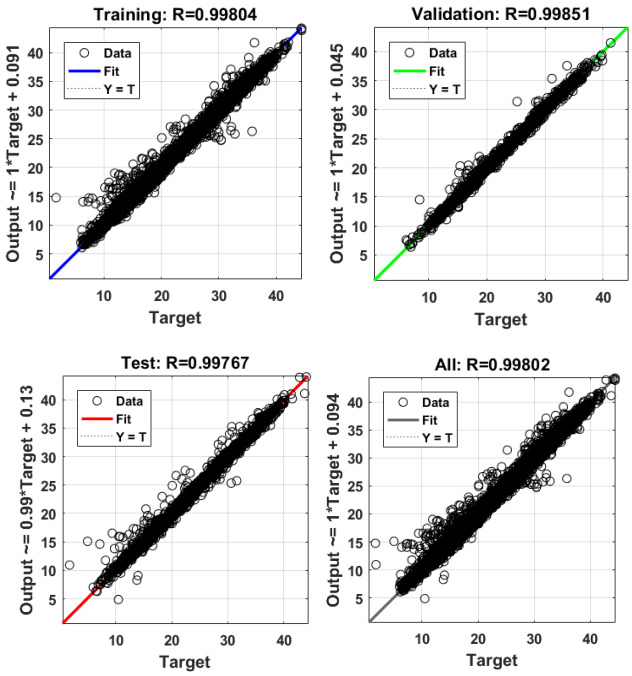

Fig. 7. Neural network performance analysis.

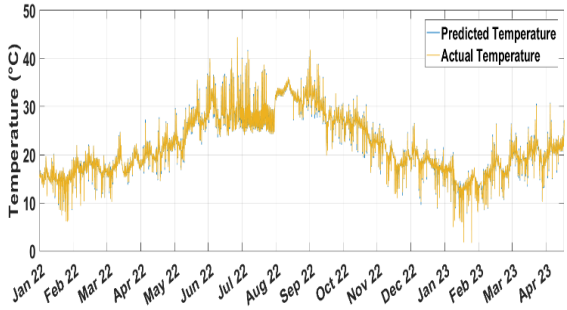

Fig. 8. Contrast between predicted and real temperatures.

4.2. Envelope Model Validation

The procedure involves selecting several consecutive days, applying the measured outside wall temperatures to the model, and comparing the simulated data with the collected data on the opposite side. The parameters of the wall model are adjusted iteratively until an error lower than a specified threshold (αmin) is achieved. This adjustment process is repeated for different days, and the average of the obtained values is calculated. The objective is to align the temperature profiles of the model as closely as achievable with the experimental temperature profiles.

Recorded thermocouple values are compared with model predictions, as shown in "Fig. 9" for three days in February and April. Despite visual differences, the profiles exhibit good agreement. Discrepancies are attributed to sensor positioning

and disturbance caused by surface-mounting sensors, which disrupt the phenomena they are supposed to record [22]. The small differences are also influenced by the sensors' positioning in the middle of the walls, affecting the accuracy of values obtained. This is particularly noteworthy since the model provides average values, while thermocouples record punctual values. The maximum difference of 1°C occurs on the flat glass of the window in February. Agreement is most pronounced in the moderate season (April).

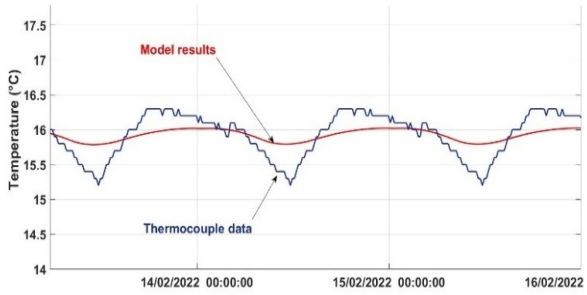

(a) Temperature's profiles north wall: extreme season (February)

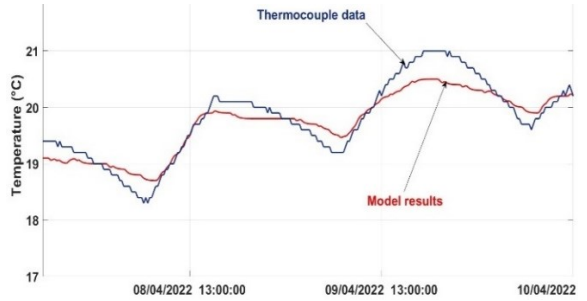

(a) Temperature's profiles north wall : moderate season (April)

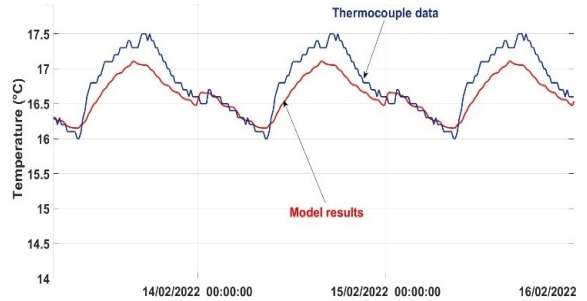

(b) Temperature's profiles south wall: extreme season (February)

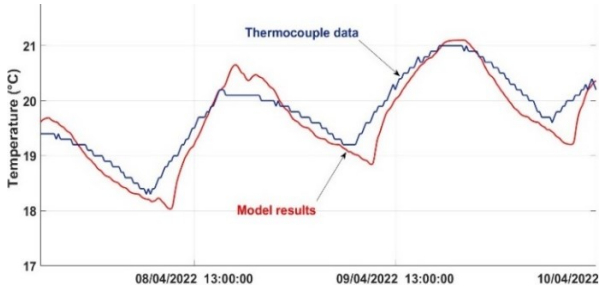

(b) Temperature's profiles south wall: moderate season (April)

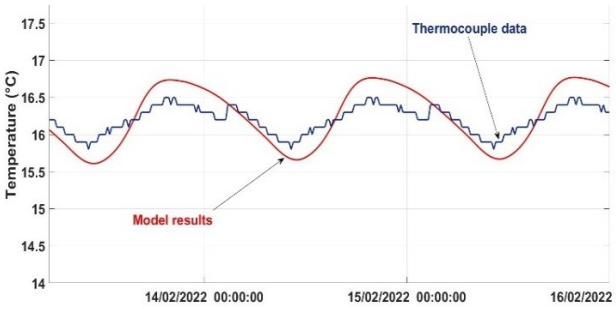

(c) Temperature's profiles west wall: extreme season (February)

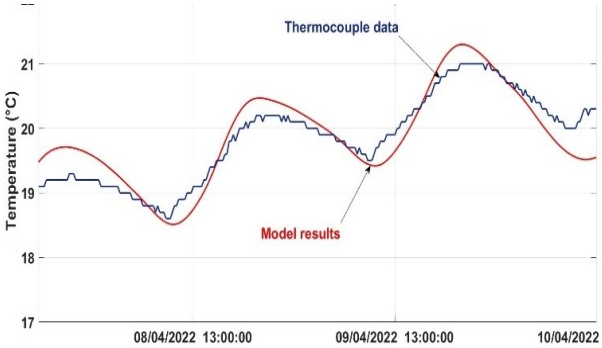

(c) Temperature's profiles west wall: moderate season (April)

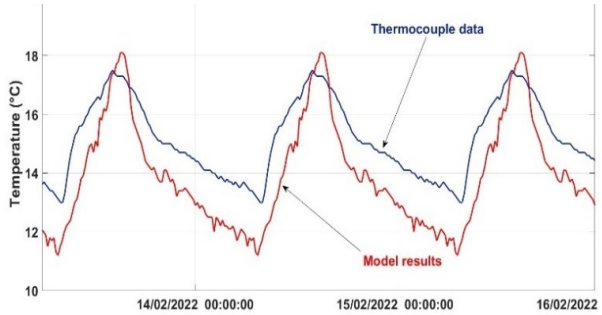

(d) Temperature's profiles of the window glass: extreme season (February)

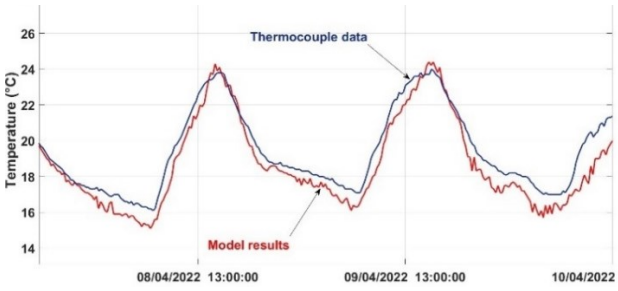

(d) Temperature's profiles of the window glass: Moderate season (April)

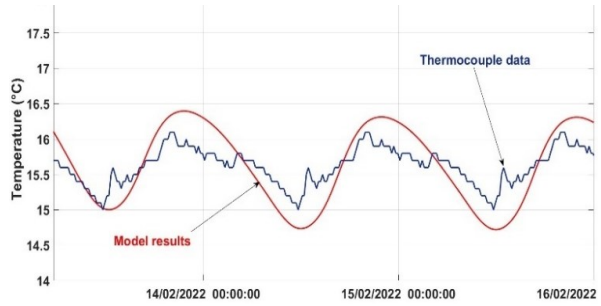

(e) Temperature's profiles east wall: extreme season (February)

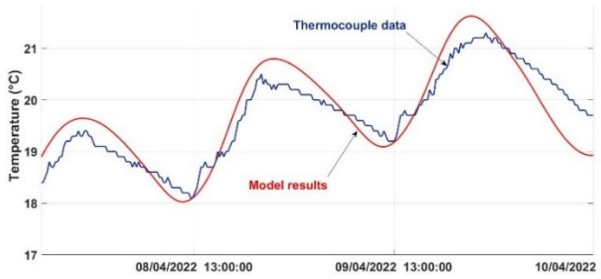

(e) Temperature's profiles east wall: moderate season (April)

Fig. 9. Envelope model validation.

4.3. Analysis of the Model's Performance

Curves in "Fig.10" show the temperatures' profiles evolution, during two consecutive days, through the different wall components envelope, and windows surface. Recorded outdoor and indoor temperature data, Text and Tin, are the current input data. Simulation of dynamic window and wall layers temperatures are illustrated to analyze their evolution by taking advantage of the fine discretization allocated by the model. The intermediate curves, between the exterior temperature and the interior temperature ones, illustrate the heat evolution through the glass of the window "Fig 10 a". Its shape is more influenced by that of the exterior than of the interior temperatures. The values obtained are also closer to the outside temperatures. This difference is more noticeable when their values begin to rise, which would generate significant losses following the increase in the thermal gradient between the interior atmosphere of the room and the windows. A zoom carried out on the glazed part of the window, highlights the effect of the fine discretization of the modelling.

The temperature curves through the thicknesses of the layers constituting the opaque surface of the east wall are illustrated in "Fig.10 b". The different layers' temperature resulting both from the temperature gradients between the inner ambient atmosphere and the external ambient ones as well as from the combined influence of the wall layers thickness and their thermo-physical characteristics. However, when the outside temperature begins to drop, from 5 p.m. to 7 p.m., the profiles obtained become nearly close for the two external layers and display temperatures higher than that of the outside. On the other hand, no changes are observed for the other layers. This behaviour is the result of the thermophysical characteristics of the external constituents' part of the wall. In addition to the insulation effect of the air gap layer (thickness 6 cm). Thus, despite the high external temperature, the difference between the indoor ambient room temperature and the internal wall face is about 1.7°C. "Figures 10 c and d" depict the different layer temperatures of the north wall and the south wall respectively. The curves obtained are for both walls at intermediate values between the inside ambient temperature of the laboratory room and those of the other walls' sides. At temperatures practically close on either side of the two walls, the difference between the two faces of the north wall is 2.5°C for a thickness of 10 cm in bricks and mortar. Whereas, for the south wall this difference is about 4.5°C for the total thickness of 4,3cm composed by gypsum plasterboards and polystyrene. On the other hand, the difference between the indoor ambient room temperature and the internal wall faces is about 2°C and 0.5°C for the north and the south wall respectively. This reflects the insulation effect of the south wall compared to the north one. The profile temperatures obtained through the west wall are depicted on "Fig.10 e". The outside temperatures registered at the corridor have a range value between those of the external temperatures registered from the external roof side and the external temperatures registered from the external wall east side. Even though it is ventilated the glass partition influences the rise of the corridor temperature. The maximum values registered are 35°C; 36°C and 32.5°C respectively. During working hours, the internal face temperature rises but the delayed effect on indoor temperatures is slightly observed in the evening. The difference between the indoor ambient room temperature and the internal wall face varies between 1°C and 2°C. Unlike all other room envelope walls, only the roof, "Fig. 10 f", has particular temperature profiles. Unlike all other room envelope walls, only the roof, shown in "Fig. 10 f", exhibits particular temperature profiles. From 11 p.m. to 9 a.m., when the outside temperature matches that of the room, the temperatures of the different layers (from the outside to the inside) decrease to become lower than or equal to the ambient temperature inside the room. These layers dissipate heat towards the outside atmosphere, cooling down without affecting the ambient temperature inside the room. During the time interval between 9 a.m. and 9 p.m., which includes the working period, only the layers of plaster, brick, and the slab reach a temperature that is slightly closer to the ambient temperature of the room.

Based on the temperature profiles observed, we can conclude a ranking of the various possible energy losses of the envelope. Contrary to common belief, the roof is not the part of the envelope through which heat loss is greatest. In fact, buildings' roofs generally receive a significant amount of solar radiation. However, the material composition and design of the roof, as well as the application of shiny and reflective materials and installed photovoltaic panels, play important roles. The former influence insulation and solar radiation reflection, respectively, while the latter contribute to a shading effect.

Likewise, if we consider the other envelope components, the north, east, and west walls, in addition to the glazed surfaces, are not in thermal equilibrium with the air inside the room, representing sources of energy loss.

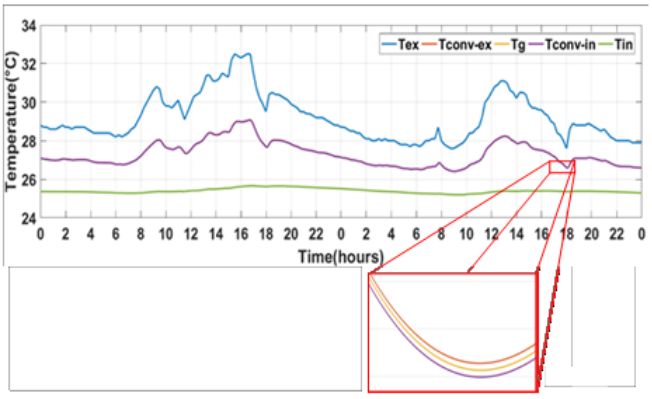

(a) East window

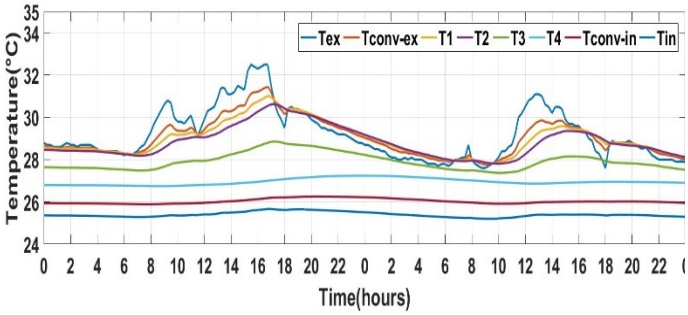

(b) East wall

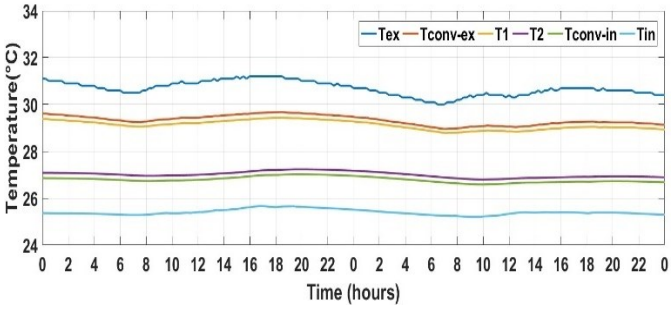

(c) North wall

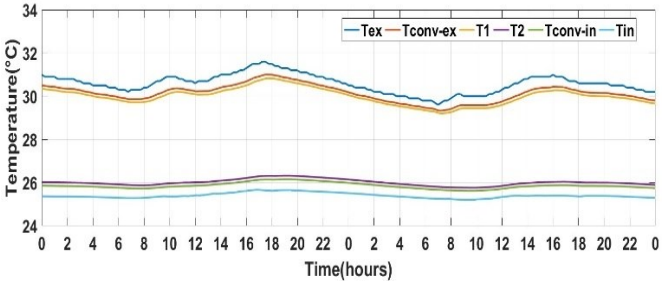

(d) South wall

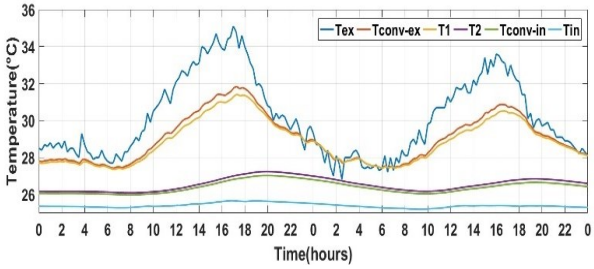

(e) West wall

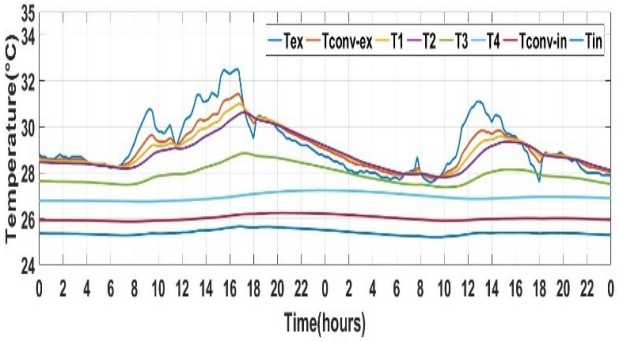

(f) Roof

Fig. 10. Temperatures profiles through the different envelope component's layers for two consecutive days.

4.4. Predicting Energy Behavior in Extreme Scenarios

In the most extreme scenario, where all loads are activated and the air conditioner operates continuously, there is a significant increase in energy consumption. The heat flow from the electrical equipment, the envelope, and the air conditioner is illustrated in "Fig. 11", while the energy balance is depicted in "Fig. 12". The heat flow generated by the air conditioner equals the sum of the internal loads and the losses through the envelope. Consequently, the room reaches thermal equilibrium, maintaining the set temperature.

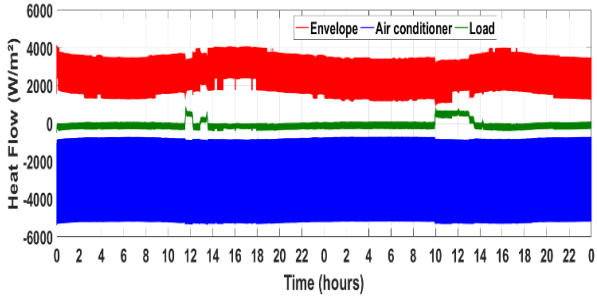

Fig. 11. Heat flow over thermal model components.

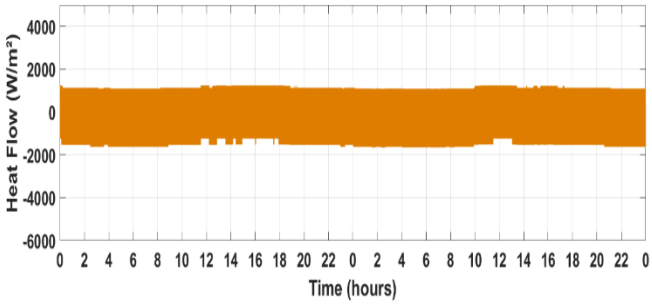

Fig. 12. Overall energy system balance.

The air conditioner energy consumption is depicted in "Fig.13". A gradual evolution marked by peaks representing the effect of load application is observed. The consumed energy reaches 10.5 kWh over a duration of two days. If we assume that the air conditioner operates solely when the internal ambient temperature reaches approximately 25°C, for a duration of 4 hours per day over a period of 5 months as indicated in "Fig 8". The annual energy consumption is expressed as 'Eq. (7)' and amounts to 3150 kWh/year. Taking

into consideration 5 months of air conditioning operation, with 20 days per month and 6 hours per day.

$$E_{AC} \approx P \cdot T_{annual\ AC\ consumption} \quad (7)$$

Where (E_{AC}) is the estimated annual energy consumed by the air conditioner in [kWh], (P) represents the power of the air conditioner for one day [kW] and ($T_{annual\ AC\ consumption}$) is the estimated duration of air conditioner operation [h].

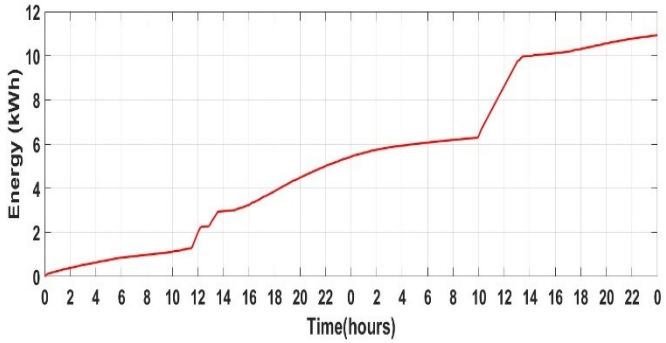

Fig. 13. Air conditioner consumption within a period of two days.

4.5. Photovoltaic Panel Integration

To reduce reliance on energy purchases from the electrical grid, we are considering the utilization of photovoltaic power. A rooftop photovoltaic system (PV) with a total power of 12.75 kWp has already been installed. Further details about the installation are provided in [23-25]. Only part of the PV installation corresponding to 2.87 kWp is considered for this study. The installed photovoltaic system, equipped with a smart inverter, is programmed to limit injected PV power onto the distribution network in accordance with European standards. This feature, known as PV curtailment, offers several advantages, including improved grid stability and reduced energy losses.

An evaluation of purchased power considering PV production is depicted in "Fig. 14". It is worth noting that the installed PV panels can fully cover all air conditioner consumption. Both scenarios are considered: when PV is curtailed according to European standards and when curtailment is not applied, allowing for the utilization of all available PV power. Even when the curtailment process is activated, all air conditioner consumption is still covered. According to "Eq. (8)", considering a solar production factor (Fps) as 5 days. The (EPV) is about 5000 kWh/year.

$$E_{PV} \approx C \cdot F_{ps} \cdot T_{annual\ Sunlight} \quad (8)$$

Where (E_{PV}) is the total energy produced over the course of a year. [kWh], (C) is the rated power of the solar panels in kilowatts peak [kWp], (F_{ps}) is the average daily sunlight hours and ($T_{annual\ Sunlight}$) is the number of hours of sunlight received in a year.

So, if the curtailed power is reduced to 60% of the available power, it is still sufficient.

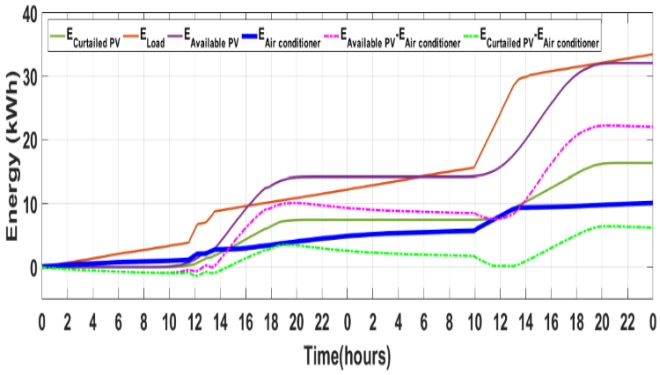

Fig. 14. Purchased power considering PV production for two days.

5. Conclusion

An integrated approach to data-driven thermal and energy management modelling of an overheated laboratory within an educational building in Tunis was carried out. Implemented predicted data in the simulation of the room model allowed both thermal and energy behavior. The room model integrate envelope, loads and air conditioner control subsystems. The effectiveness of the methodology, which relies on input from on-site temperature measurements, is validated. The heat loss from the envelope was determined through an in-depth study of the thermal behavior of the walls. Analysis of typical days revealed a high consumption of air conditioning. To address this, a proposed renewable energy system was installed to offset the cooling energy required, ensuring independence from the national electric grid. The study findings indicate that the predictive model exhibits a slight error margin of approximately 2%. Additionally, the envelope model demonstrates an error of less than 1°C, except for the glass side where it reaches 1°C on the flat glass of the window. Moreover, the predicted air conditioning consumption derived from the proposed model provides compelling evidence that the installed PV system, despite the curtailment mode of PV functioning, adequately meets the energy demand, ensuring coverage.

Acknowledgements

This work was supported by the Tunisian Ministry of Higher Education and Scientific Research under Grant LETTM-LR01ES07 and LSE-ENIT-LR 11ES15, the research common services unit MICROGRID Platform (USCR-MGP), Research and Development Program: Project AmEE under reference: 20/ PRD-21 and by the project "Development of an Intelligent, Sustainable and Autonomous Cold Room Powered by Photovoltaic Panels (Code T3P3) ", supported by the ARESSE component of the environmental action support program "Tunisie Verte & Durable", funded by the European Union.

Author Contributions

A.S. Cherif was responsible for the conceptualization, validation, resources, data curation, software development, project administration, and original draft preparation. A.S.

Cherif and S. Skander-Mustapha jointly contributed to the methodology, formal analysis, investigation, review and editing, and visualization. I. Slama Belkhodja supervised the work and contributed to funding acquisition and review and editing. All authors have read and agreed to the published version of the manuscript.

Conflict of Interest

The authors declare no potential conflicts of interest with respect to the research, authorship, and/or publication of this article.

References

[1] H. Fu, J.-C. Baltazar, and D. E. Claridge, "Review of developments in whole-building statistical energy consumption models for commercial buildings," Renewable and Sustainable Energy Reviews, vol. 147, p. 111248, 2021. doi: 10.1016/j.rser.2021.111248.

[2] N. Mdini, S. Skander-Mustapha, and I. Slama-Belkhodja, "Design of passive power filters for battery energy storage system in grid connected and islanded modes," SN Applied Sciences, vol. 2, no. 5, p. 933, 2020. doi: 10.1007/s42452-020-2747-7.

[3] S. Skander-Mustapha and I. Slama-Belkhodja, "Energy management of rooftop PV system including battery storage: Case study of ENIT building," International Conference on Electrical and Information Technologies, Rabat, Morocco, pp. 1–6, Mar. 2020.

[4] M. S. Geraldi, A. P. Melo, R. Lamberts, E. Borgstein, A. Y. G. Yukizaki, A. C. B. Maia, J. B. Soares, and A. dos Santos Junior, "Assessment of the energy consumption in non-residential building sector in Brazil," Energy and Buildings, vol. 273, p. 112371, 2022. doi: 10.1016/j.enbuild.2022.112371.

[5] X. Zhou, Y. Mei, L. Liang, H. Mo, J. Yan, and D. Pan, "Modeling of occupant energy consumption behavior based on human dynamics theory: A case study of a government office building," Journal of Building Engineering, vol. 58, p. 104983, 2022. doi: 10.1016/j.jobe.2022.104983.

[6] V. Gupta and C. Deb, "Energy retrofit analysis for an educational building in Mumbai," Sustainable Futures, vol. 4, p. 100096, 2022. doi: 10.1016/j.sftr.2022.100096.

[7] Y. Bae, S. Bhattacharya, B. Cui, S. Lee, Y. Li, L. Zhang, P. Im, V. Adetola, D. Vrabie, M. Leach, and T. Kuruganti, "Sensor impacts on building and HVAC controls: A critical review for building energy performance," Advances in Applied Energy, vol. 4, p. 100068, 2021. doi: 10.1016/j.adapen.2021.100068.

[8] B. Delač, B. Pavković, K. Lenić, and D. Mađerić, "Integrated optimization of the building envelope and the HVAC system in nZEB refurbishment," Applied Thermal Engineering, vol. 211, p. 118442, 2022. doi: 10.1016/j.applthermaleng.2022.118442.

[9] M. A. Kallioğlu, A. Sharma, V. Chinnasamy, R. Chauhan, and T. Singh, "Optimum insulation thickness assessment of different insulation materials for mid-latitude steppe and desert climate (BSH) region of India," Materials Today: Proceedings, vol. 44, pp. 4421–4424, 2021. doi: 10.1016/j.matpr.2020.10.590.

[10] A. Allik, S. Muiste, and H. Pihlap, "Smart meter data analytics for occupancy detection of buildings with renewable energy generation," 9th International Conference on Renewable Energy Research and Application (ICRERA), Glasgow, UK, pp. 284–291, Sep. 2020.

[11] Z. Wei and J. Calautit, "Investigation of the effect of the envelope on building thermal storage performance under model predictive control by dynamic pricing," Smart Energy, vol. 6, p. 100068, 2022. doi: 10.1016/j.segy.2022.100068.

[12] N. Mendes, G. H. C. Oliveira, H. X. Araújo, and L. S. Coelho, "A Matlab-based simulation tool for building thermal performance analysis," Eighth International IBPSA Conference, Eindhoven, Netherlands, pp. 1–8, Aug. 2003.

[13] B. Duzgun, R. Bayindir, and H. I. Bulbul, "Policy instruments to promote the use of renewable energy for residential heating and cooling: A case of Turkey," 10th International Conference on Renewable Energy Research and Application (ICRERA), Istanbul, Turkey, Sep. 2021.

[14] H. Bakiri, H. Maziku, N. Mvungi, and N. Hamis, "Towards the establishment of robust load forecasting mechanism in Tanzania grid: Effect of air temperature and daytime on electricity consumption in residential buildings," International Journal of Smart Grid, vol. 5, no. 1, 2021. doi: 10.20508/ijsmartgrid.v5i1.159.g140.

[15] M. Kingsley-Amaehule, R. Uhunmwangho, N. Nwazor, E. S. Mbonu, and K. E. Okedu, "Investigation of the impact of soot on the efficiency of solar panels using a smart intelligent monitoring system," International Journal of Smart Grid, vol. 7, no. 1, pp. 1–13, 2023. doi: 10.20508/ijsmartgrid.v7i1.269.g255.

[16] J. A. Thomas, "Prediction of heat demand for building energy managers: An IoT and control perspective," 8th International Conference on Smart Grid (icSmartGrid), Paris, France, pp. 29–36, June 2020.

[17] I. Colak, R. Bayindir, and S. Sagiroglu, "The effects of the smart grid system on the national grids," 8th International Conference on Smart Grid (icSmartGrid), Paris, France, June 2020.

[18] F. Qi, X. Jin, Y. Mu, H. Jia, X. Xu, X. Yu, and T. Wang, "Model predictive control approach for building microgrid considering dynamic thermal characteristics of building," Energy Procedia, vol. 105, pp. 2785–2790, 2017. doi: 10.1016/j.egypro.2017.03.599.

[19] F. Mutasim Baba, M. Haj Hussein, S. Saleh, M. Baba, and J. Awad, "Spatially resolved indoor overheating evaluation using microscale meteorological simulation as input for building simulation: Opportunities and

limitations," Building and Environment, vol. 245, p. 110871, 2023. doi: 10.1016/j.buildenv.2023.110871.

[20] C. Schünemann, A. Ziemann, and V. Goldberg, "Building parameters that influence overheating of apartment buildings in a temperate climate in Southern Europe," City and Environment Interactions, vol. 20, p. 100122, 2023. doi: 10.1016/j.cacint.2023.100122.

[21] U. Y. A. Tettey and L. Gustavsson, "Energy savings and overheating risk of deep energy renovation of a multi-storey residential building in a cold climate under climate change," Energy, vol. 202, p. 117578, 2020. doi: 10.1016/j.energy.2020.117578.

[22] S. K. Singh, M. K. Yadav, R. Sonawane, S. Khandekar, and K. Muralidhar, "Estimation of time-dependent wall heat flux from single thermocouple data," International Journal of Thermal Sciences, vol. 115, pp. 1–15, 2017. doi: 10.1016/j.ijthermalsci.2017.01.010.

[23] M. Dellaly, S. Skander-Mustapha, and I. Slama-Belkhodja, "Optimization of a residential community's curtailed PV power to meet distribution grid load profile requirements," Renewable Energy, vol. 218, p. 119342, 2023. doi: 10.1016/j.renene.2023.119342.

[24] M. Dellaly, S. Moussa, S. Skander-Mustapha, and I. Slama-Belkhodja, "Analysis and assessment of a commercial microgrid laboratory platform," IMACS TC1 Conference, Cham: Springer, pp. 399–409, 2021.

[25] M. Dellaly, S. Skander-Mustapha, and I. Slama-Belkhodja, "Data-driven emulation of a peer-to-peer energy exchanged for interconnected residential nanogrids," IEEE International Conference on Electrical Sciences and Technologies in Maghreb, Tunis, Tunisia, pp. 1–7, Oct. 2022.